Article

J. Biol. Regul. Homeost. Agents. 2024; 38(5): 4375–4385
https://doi.org/10.23812/j.biol.regul.homeost.agents.20243805.347

NRF2 Upregulates *GPX2* to Inhibit Ferroptosis and Enhance Immune Escape of Melanoma

Lihua Wu[1,†], Min Li[2,†], HSIN-YU HUNG[3,4,*]

[1]Department of Pathology, The 2nd Affiliated Hospital of Harbin Medical University, 150086 Harbin, Heilongjiang, China
[2]Department of Dermatology, Taihe Hospital, Hubei University of Medicine, 442000 Shiyan, Hubei, China
[3]Depatment of Plastic Surgery, Meishiti Fashion Medical Beauty Clinic, 105401 Taipei, Taiwan
[4]School of Chinese Medicine, College of Chinese Medicine, China Medical University, 406040 Taichung, Taiwan
*Correspondence: hongxinyu_hxinyu@163.com (HSIN-YU HUNG)
[†]These authors contributed equally.
Published: 1 May 2024

Background: Melanoma is the deadliest form of skin malignant tumor, with NFE2 like bZIP transcription factor 2 (*NRF2*) and glutathione peroxidase 2 (*GPX2*) implicated in its progression. In this report, we explored the interplay of *NRF2* and *GPX2* in melanoma using both *in vitro* and *in vivo* approaches.

Methods: B16 cells were transfected with *NRF2* overexpression plasmid and/or small interfering RNA against GPX2 (Si-*GPX2*) plasmid and treated with erastin to induce ferroptosis. Quantitative real-time polymerase chain reaction (qRT-PCR) was used to determine transfection efficiency. To investigate immune escape, B16 cells were co-cultured with $CD8^+$ T cells, and mice bearing subcutaneous xenograft tumor were established and injected with programmed cell death 1 (PD-1) or CD274 molecule (PD-L1) antibody. Cell viability, colony formation, and expressions of GPX2 and PD-L1 were analyzed by Cell Counting Kit-8, colony formation, and western blot assays. Levels of ferrous iron (Fe^{2+}), malondialdehyde (MDA), lipid peroxidation, and reactive oxygen species (ROS) were measured. $CD8^+$ T cell apoptosis and infiltration were determined by flow cytometry and immunohistochemistry.

Results: *NRF2* overexpression increased viability, colony formation, and *GPX2*/PD-L1 expression ($p < 0.05$), but reduced levels of Fe^{2+}, MDA, lipid peroxidation, and ROS in erastin-treated B16 cells, while *GPX2* knockdown decreased colony formation and PD-L1 expression, but increased levels of Fe^{2+} and lipid peroxidation ($p < 0.01$). Following co-culture, $CD8^+$ T cell apoptosis was promoted by *NRF2* overexpression, but inhibited by *GPX2* knockdown ($p < 0.01$). *GPX2* knockdown reversed the effects of *NRF2* overexpression on the above indices ($p < 0.01$). In mice with subcutaneous xenograft tumor, *NRF2* overexpression decreased $CD8^+$ T cell infiltration, which was restored by blocking PD-1 and PD-L1 ($p < 0.01$).

Conclusion: *NRF2* upregulates *GPX2* to inhibit ferroptosis and enhance immune escape of melanoma, unveiling a previously unknown therapeutic target to improve the efficacy of melanoma immunotherapy.

Keywords: NFE2 like bZIP transcription factor 2; glutathione peroxidase 2; immune escape; ferroptosis; melanoma

Introduction

Melanoma is the deadliest type of skin malignant tumor. It is caused by malignant transformation of epidermal melanocytes and has the ability to spread and metastasize to distant sites [1], with increasing trends of morbidity and mortality worldwide. As predicted by the International Agency for Research on Cancer (IARC), melanoma morbidity and mortality will increase by 78% and 73% [2]. In clinical practice, even though surgery has high efficacy in treating many melanoma patients with localized lesions, it fails to cure patients with metastatic melanoma [3]. Of note, improvement in melanoma outcomes has been observed through recent advances in targeted therapy and immunotherapy [4]. The activation of $CD8^+$ T cells to suppress immune checkpoints causes melanoma ferroptosis [5]. Immunotherapy enhances lipid peroxidation and activates ferroptosis as a cytotoxic pathway in melanoma cells via activation of $CD8^+$ T cells [6]. Moreover, DNA damage regulates ferroptosis in melanoma cells. For example, overexpressed TYRO3 is involved in anti- programmed cell death 1 (PD-1)/CD274 molecule (PD-L1) resistance through inhibition of tumor ferroptosis [7,8]. Overall, it has been found that higher effectiveness in immunotherapy can be achieved by triggering ferroptosis in cells.

NFE2 like bZIP transcription factor 2 (*NRF2*) encodes a transcription factor which mediates antioxidant response elements (ARE)-containing genes [9]. The importance of *NRF2* in the oxidative stress response has been reported in considerable studies [10–12]. In addition, *NRF2* is a vital regulatory factor in the immune response [13,14]. For example, immune-responsive gene 1 protects against liver

Journal of
BIOLOGICAL REGULATORS
and Homeostatic Agents

injury via *NRF2* activation and reactive oxygen species (ROS) inhibition [15]. It is also worth mentioning that *NRF2* mediates tumor immune escape [16,17]. Immune escape occurs when tumor cells evade the detection and attack of immune system through antigenic deletion, immunological suppression, tumor cell leakage, the absence of costimulatory signals on the tumor cell surface, or the antiapoptotic properties of tumor cells, allowing them to survive and proliferate [18,19]. However, the impact of *NRF2* upon immune escape in melanoma has not been reported.

Glutathione peroxidase 2 (*GPX2*) belongs to the glutathione peroxidase family, where members inhibit oxidative damage in cells through catalyzing the reduction of organic hydroperoxides and hydrogen peroxide via glutathione [20]. Ferroptosis, a type of programmed cell death, results from iron-induced lipid ROS accumulation which incurs intracellular oxidative stress [21]. *GPX2* displays antioxidant activity in ferroptosis to protect the cell against oxidative damage and has been acknowledged as a ferroptosis-related gene [22]. Ferroptosis escape is a determinant of melanoma metastasis and immune escape [23]. Additionally, *GPX2* is a metabolic driver for immune checkpoint inhibitor responses in tumors [24]. Though an intimate correlation between *GPX2* expression and *NRF2* activation exists in a variety of cancers [25], the relationship between *NRF2* and *GPX2* is obscure in melanoma, which is the core of this study.

Therefore, we investigated the involvement of *NRF2* and *GPX2* in ferroptosis and melanoma immune escape using *in vivo* and *in vitro* assays.

Materials and Methods

Cell Culture and Transfection

The mouse melanoma cell line B16 (191731, Zhongke Quality Inspection Biotechnology Co., Ltd., Beijing, China) and $CD8^+$ T cells (BFN60810807, Bluefcell, Shanghai, China) supplemented with RPMI-1640 medium (R8758, Sigma-Aldrich, St. Louis, MO, USA), 10% fetal bovine serum (FBS, F2442, Sigma-Aldrich, St. Louis, MO, USA) and 1% penicillin/streptomycin (V900929, Sigma-Aldrich, St. Louis, MO, USA) were cultured in an incubator (37 °C, 5% CO_2). All cells were free of mycoplasma contamination.

For transfection, the full sequence of *NRF2* (**Supplementary material 1**) was assembled into pcDNA3.1 vectors (OE-*NRF2*, VT1001, YouBio, Changsha, China), with empty vectors as negative control (OE-NC). All sequences of small interfering RNA against *GPX2* (small interfering RNA against GPX2 (Si-*GPX2*), sense: 5′-CCUCAGCAUUCCCUUGAUATT-3′; antisense, 5′-UAUCAAGGGAAUGCUGAGGTT-3′) and its negative control siRNA (*Si-NC*, sense: 5′-UUCUCCGAACGUGUCACGUTT-3′; antisense: 5′-AGCUGACACGUUCGGAGAATT-3′) were obtained from GenePharma (A04001, Shanghai, China). Lipofectamine 3000 Reagent (L3000001, ThermoFisher, Waltham, MA, USA) was used to transfect the above plasmids into B16 cells (1×10^4 cells/well in 96-well plates) at 70–90% confluence. After dilution of Lipofectamine 3000 Reagent and vectors/siRNAs in Opti-MEM™ (31985062, ThermoFisher, Waltham, MA, USA), the mixture of vectors with 0.2 µL P3000 Reagent and vectors/siRNAs was incubated in diluted Lipofectamine 3000 Reagent at room temperature (RT) for 10 min. Then, cell culture (96-well plates) with the complexes was performed at 37 °C for 48 h. Finally, transfection efficiency was determined by quantitative real-time polymerase chain reaction (qRT-PCR).

qRT-PCR

Total RNA extraction and reverse transcription into the first-strand complementary DNA (cDNA) were accomplished by Trizol Reagent (T9424, Sigma-Aldrich, St. Louis, MO, USA) and the Revert Aid cDNA synthesis kit (K1622, Solarbio, Beijing, China), respectively. cDNA was submitted to qRT-PCR by Fast SYBR™ Green Master Mix (4385612, ThermoFisher, Waltham, MA, USA) in a real-time PCR instrument (CFX96 Touch, Bio-Rad Laboratories, Inc., Hercules, CA, USA) under the conditions: 95 °C for 2 min, then 40 cycles at 95 °C for 3 s and 60 °C for 30 s. Data were processed by the $2^{-\Delta\Delta Ct}$ method [26], and glyceraldehyde-phosphate dehydrogenase (*GAPDH*) served as the internal control.

The following primer sequences were used in these experiments: *NRF2* forward primer (F), 5′-CTTGGAGTAAGTCGAGAAGTA-3′, reverse primer (R), 5′-CATCTACAAACGGGAATG-3′; *GPX2* F, 5′-AGTCCTTCTATGACCTCAGTG-3′, R, 5′-GGACGGACATACTTGAGA-3′; *GAPDH* F, 5′-AGAAGGCTGGGGCTCATTTG-3′, R, 5′-AGGGGCCATCCACAGTCTTC-3′.

Cell Treatment

Erastin (E7781, Sigma-Aldrich, St. Louis, MO, USA) in dimethyl sulfoxide (DMSO, D1435, Sigma-Aldrich, St. Louis, MO, USA) was diluted in medium to 5 µM concentration for treating B16 cells (24 h) as per the previous study [27].

Cell Counting Kit-8 (CCK-8) Assay

B16 cells in 96-well plates (5×10^3 cells/well) were cultured for 24/48/72 h following transfection. Next, 10 µL CCK-8 reagent (ab228554, Abcam, Cambridge, UK) was added to each well for a 4-h incubation in darkness. Absorbance at 460 nm of each well was measured using an enzyme-linked immunosorbent assay (ELISA) reader (Bio-Rad 680, Bio-Rad Laboratories, Inc., Hercules, CA, USA).

Colony Formation Assay

200 µL cells (1×10^3 cells/well) were seeded into 6-well plates and cultured for two weeks. When the colony was formed, the medium was discarded. Cell fixation (4% paraformaldehyde, P1110, Solarbio, Beijing, China) and staining (Giemsa, G1010, Solarbio, Beijing, China) were performed for 15 min at RT. After cell washing with phosphate buffered solution (PBS, P1020, Solarbio, Beijing, China), cell colony observation and counting were conducted utilizing a BX53F microscope (Olympus, Tokyo, Japan). The colony formation rate was calculated by the equation [number of cell colonies ($\geq$50 per colony)/total cell number] $\times$ 100%, and normalized to the control or the OE-NC+Si-NC group.

Iron Assay

An iron assay kit (ab83366, Abcam, Cambridge, UK) was employed to measure the ferrous iron (Fe^{2+}) level in B16 cells. Briefly, the supernatant was collected by centrifugation after cell homogenization in cold Iron Assay Buffer. Thereafter, 2–50 µL samples were added into each well and left in 5 µL Iron Assay Buffer at 37 °C for 30 min, followed by 1-h culture with 100 µL Iron Probe in darkness. The absorbance of each well at 593 nm was measured by an ELISA reader (Bio-Rad 680, Bio-Rad Laboratories, Inc., Hercules, CA, USA).

Determination of Malondialdehyde (MDA)

A Lipid Peroxidation MDA Assay Kit (S0131S, Beyotime, Shanghai, China) was used to detect MDA level in B16 cells. Cells were first homogenized by PBS. Then, 0.1 mL samples were mixed with 0.2 mL MDA determination working solution, heated in boiling water for 15 min, cooled to RT, and centrifuged (1000 $\times$g, 10 min). Supernatant was collected and absorbance at 532 nm was determined on an ELISA reader (Bio-Rad 680, Bio-Rad Laboratories, Inc., Hercules, CA, USA).

C11-BODIPY Staining

Levels of lipid peroxidation in B16 cells were evaluated by BODIPY™ 581/591 C11 (D3861, ThermoFisher, Waltham, MA, USA). Briefly, C11-BODIPY was added to the medium to 2 µM concentration, and incubated with the cells (30 min, 37 °C). The fluorescence signal was observed under a CX31 microscope (Olympus, Tokyo, Japan) at $\times$200 magnification using 545/40 nm excitation filter and 620/40 nm emission filter [28].

Measurement of ROS

Reactive Oxygen Species Assay Kit (S0033S, Beyotime, Shanghai, China) was used to detect ROS level in B16 cells. Briefly, 2 µM 2,7-dichlorodihydrofluorescein diacetate (DCFH-DA) in serum-free medium was co-incubated with treated B16 cells (20 min, 37 °C). After washing three times with serum-free culture medium, cells were resuspended in PBS, and the cell fluorescence signal was detected by a CX31 microscope ($\times$200 magnification, Olympus, Tokyo, Japan).

Western Blot

Proteins from B16 cells were extracted with radioimmunoprecipitation assay buffer (R0010, Solarbio, Beijing, China) and then immersed in boiling water for 5 min. Protein concentration was determined with a bicinchoninic acid protein assay kit (23227, ThermoFisher, Waltham, MA, USA). Proteins were separated in 10% separation gel (P0670, Beyotime, Shanghai, China) by sodium dodecyl sulfate-polyacrylamide gel electrophoresis and transferred onto the polyvinylidene fluoride membrane (YA1701, Solarbio, Beijing, China). Following blocking with 5% non-fat milk (D8340, Solarbio, Beijing, China) diluted by Tris Buffered Saline and Tween-20 (T1085, Solarbio, Beijing, China) (1 h, RT), the membrane was incubated with primary antibodies (overnight, 4 °C), and then cultured with horseradish peroxidase (HRP)-conjugated secondary antibodies (1 h, RT). After treatment with enhanced chemiluminescence (ECL) reagent (FP300, ABP Biosciences, Rockville, MD, USA), analysis of band signals was performed on 5200 imaging system (Tanon, Shanghai, China), followed by quantitative analysis with GAPDH as the internal reference using ImageJ software (1.52s version, National Institutes of Health, Bethesda, MD, USA).

The antibodies used were obtained from Abcam (Cambridge, UK), including GPX2 (ab137431, 22 kDa, 1:1000), PD-L1 (ab213480, 33 kDa, 1:1000), GAPDH (ab181602, 36 kDa, 1:10,000), and anti-rabbit Immunoglobulin G (IgG) (ab99697, 1:1000).

Flow Cytometry

B16 cells (1×10^5) and $CD8^+$ T cells (5×10^5) were co-cultured at a ratio of 1:5 for 24 h. With $CD8^+$ T cells in the lower chamber of transwell (140620, ThermoFisher, Waltham, MA, USA) and B16 cells in the upper chamber, $CD8^+$ T cell apoptosis was tested by the Annexin-V-fluorescein isothiocyanate (FITC) Apoptosis Detection Kit (K201-100, Biovision, Milpitas, CA, USA). Digested cells were mixed with Annexin-V-FITC, Propidium Iodide (PI), and 4-(2-hydroxyerhyl) piperazine-1-erhanesulfonic acid (HEPES) buffer solution (PB180325, Procell, Wuhan, China) at a ratio of 1:2:50 in Annexin-V-FITC/PI staining solution. Cells (1×10^6 cells/100 µL) in staining solution were incubated (15 min, RT) with 1 mL HEPES buffer solution. FITC and PI fluorescence were detected (525 and 620 nm, respectively) in Attune NxT flow cytometer (Thermo Fisher, Waltham, MA, USA) to evaluate cell apoptosis, followed by data analysis using Cell Quest software (version 5.1, BD Biosicences, San Diego, CA, USA).

Journal of
BIOLOGICAL REGULATORS
and Homeostatic Agents

In Vivo Xenograft Assay

All animal experiments were approved by the Zhejiang Province Center for Laboratory Animals, Institutional of Animal Care and Use Committee (No. ZJCLA-IACUC-20020175).

C57BL/6 mice (n = 24, 18 ± 2 g, 6 weeks old, male) were adapted to a specific pathogen-free environment (22–24 °C, 50–60% humidity, circadian cycle) for a week, and divided into four groups: OE-NC, OE-NRF2, OE-NRF2+anti-PD-1, and OE-NRF2+anti-PD-L1. For establishing subcutaneous xenograft tumor model, as described in a previous study [29], 5×10^6 B16 cells transfected with OE-NC or OE-NRF2 were resuspended in PBS and injected subcutaneously into the left flank subscapular of mice. Afterwards, mice in OE-NRF2+anti-PD-1 and OE-NRF2+anti-PD-L1 groups were injected with PD-1 antibody (ab52587, Abcam, Cambridge, UK), or PD-L1 antibody (ab205921, Abcam, Cambridge, UK). Finally, tumor size was measured sequentially in each mouse by a digital caliper and calculated as per the formula: 0.5 × length × width^2. When the mice tumor volumes are ≤2000 mm^3 and d ≤20 mm, mice were anesthetized by 0.9% sodium pentobarbital (50 mg/kg body weight, P3761, Haoran Bio-Pharma, Shanghai, China). After collecting tumors from xenografts, mice were euthanized by cervical dislocation.

Immunohistochemistry (IHC)

After fixing with 4% paraformaldehyde for 48 h, tumor tissue was dehydrated and permeabilized with alcohol and xylene (E809063, X820585, MACKLIN, Shanghai, China). Paraffin-embedded tissues were sliced into 6 μm-thick sections. The sections were dewaxed, and soaked in different concentrations of alcohol and then stained.

For IHC staining, the sections were immersed in PBS containing Triton X-100 and 30% H_2O_2 (T8787, 323381, Sigma-Aldrich, St. Louis, MO, USA) (30 min, darkness, RT), treated with antigen repair buffer (C1031, Solarbio, Beijing, China) (20 min, 37 °C), soaked in 5% goat serum (SL038, Solarbio, Beijing, China) (30 min, RT), and incubated with CD8 primary antibody (MA5-17006, ThermoFisher, Waltham, MA, USA) (overnight, 4 °C) and HRP-conjugated secondary antibody goat anti-rat IgG (PA1-84710, 1:200, ThermoFisher, Waltham, MA, USA) (30 min, 37 °C). DAB Horseradish Peroxidase Color Development Kit (P0203, Beyotime, Shanghai, China) was employed to develop the sections. After hematoxylin staining, dehydration, and blockage, the sections were observed under a CX31 microscope (×100 magnification, Olympus, Tokyo, Japan).

Statistical Analysis

All data were analyzed by GraphPad (version 8.0, GraphPad Software, San Diego, CA, USA). Data were presented as mean ± standard deviation. Two-group and multi-group comparisons were performed by paired *t*-test and one-way analysis of variance (Tukey test for post-hoc analysis), respectively. Significant variance was indicated at $p < 0.05$.

Results

NRF2 Overexpression Elevated Viability and Colony Formation in Erastin-Treated B16 Cells

To assess the influence of *NRF2* on B16 cells, *NRF2*-overexpressing cells were successfully constructed, as shown by increased expression of *NRF2* following transfection (Fig. 1A, $p < 0.001$). In addition, erastin was applied to induce ferroptosis in B16 cells. *NRF2*-overexpressing cells had higher viability at 24/48/72 h (Fig. 1B, $p < 0.05$) and stronger colony formation ability (Fig. 1C,D, $p < 0.001$), compared to OE-NC-transfected cells. Thus, these results demonstrated that *NRF2* overexpression increased viability and colony formation in erastin-treated B16 cells.

NRF2 Overexpression Inhibited Ferroptosis and Upregulated GPX2 Protein Expression in Erastin-Treated B16 Cells

Based on the above results, we concluded that *NRF2* overexpression enhanced the proliferation of erastin-treated B16 cells, and whether *NRF2* was involved in erastin-induced ferroptosis remained unknown. To evaluate ferroptosis level, we measured Fe^{2+} content. *NRF2* overexpression decreased Fe^{2+} level in erastin-treated B16 cells (Fig. 1E, $p < 0.001$). In addition, levels of MDA, lipid peroxidation, and ROS were also used to assess ferroptosis. A reduced MDA level was observed in erastin-treated B16 cells following *NRF2*-overexpressing vector transfection (Fig. 1F, $p < 0.001$), while fluorescence signals labeling lipid peroxide (Fig. 1G,H, $p < 0.001$) and ROS (Fig. 2A,B, $p < 0.001$) were also lower in erastin-treated B16 cells. These results indicated that *NRF2* overexpression inhibited erastin-induced ferroptosis in B16 cells. Interestingly, GPX2 expression was upregulated following *NRF2* overexpression in erastin-treated B16 cells (Fig. 2C,D, $p < 0.001$), suggesting a positive relationship of *NRF2* and GPX2 in ferroptosis of B16 cells.

GPX2 Knockdown Reversed the Effects of NRF2 Overexpression on Proliferation, Ferroptosis, and PD-L1 Expression in Erastin-Treated B16 Cells

We found that *NRF2* overexpression enhanced colony formation and inhibited ferroptosis in erastin-treated B16 cells. To study the relationship of *NRF2* and *GPX2*, we successfully knocked down *GPX2* in B16 cells, as shown by decreased *GPX2* expression following Si-*GPX2* transfection (Fig. 3A, $p < 0.001$). As shown in Fig. 3B–F, *GPX2* knockdown reduced colony formation (Fig. 3B,C, $p < 0.01$), increased Fe^{2+} level (Fig. 3D, $p < 0.001$), and enhanced lipid peroxidation (Fig. 3E,F) in B16 cells following erastin treatment, which was offset by *NRF2* overexpres-

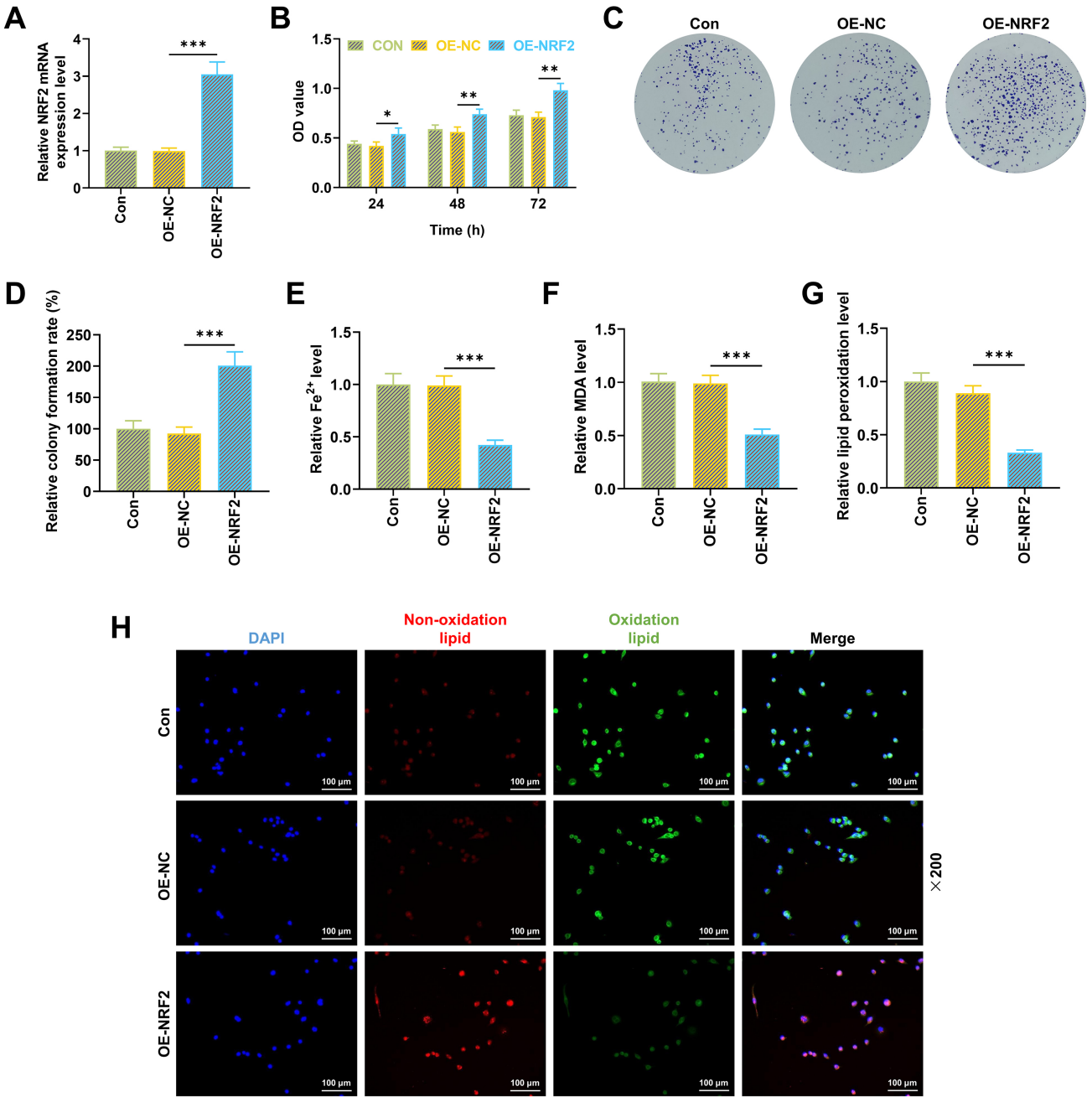

Fig. 1. Effects of *NRF2* overexpression on viability, colony formation, the level of Fe^{2+} and MDA, and lipid peroxidation in erastin-treated B16 cells. (A) Transfection efficiency after B16 cells was transfected with *NRF2*-overexpressing vectors (qRT-PCR, *GAPDH* as the internal control). (B–H) After 24-h treatment with 5 μM erastin, cell viability at 24/48/72 h (CCK-8 assay) (B), cell colonies (colony formation assay) (C,D), Fe^{2+} and MDA levels (specific kits) (E,F), and lipid peroxidation (C11-BODIPY staining) (G,H) were measured (×200 magnification, scale bar: 100 μm). n = 3. $^{*}p < 0.05$, $^{**}p < 0.01$, $^{***}p < 0.001$. *NRF2*, NFE2 like bZIP transcription factor 2; Fe^{2+}, ferrous iron; MDA, malondialdehyde; GAPDH, glyceraldehyde-phosphate dehydrogenase; NC, negative control; qRT-PCR, quantitative real-time polymerase chain reaction; CCK-8, Cell Counting Kit-8.

sion (Fig. 3B–F, $p < 0.01$). Meanwhile, *GPX2* knockdown also reversed the effects of *NRF2* overexpression on promoting colony formation (Fig. 3B,C, $p < 0.01$), and suppressing Fe^{2+} level (Fig. 3D, $p < 0.001$) and lipid peroxidation (Fig. 3E,F, $p < 0.001$) in erastin-treated B16 cells. These results demonstrated that *NRF2* affects proliferation and ferroptosis of B16 cells by upregulating *GPX2*. As ferroptosis can mediate the effect of anti-PD-1 immunotherapy on melanoma [30], we investigated whether *NRF2*/*GPX2* affected PD-1-induced immune escape in B16 cells. First, PD-L1 was highly expressed in NRF2-overexpressing B16 cells (Fig. 4A,B, $p < 0.001$) after erastin treatment, which

Journal of
BIOLOGICAL REGULATORS
and Homeostatic Agents

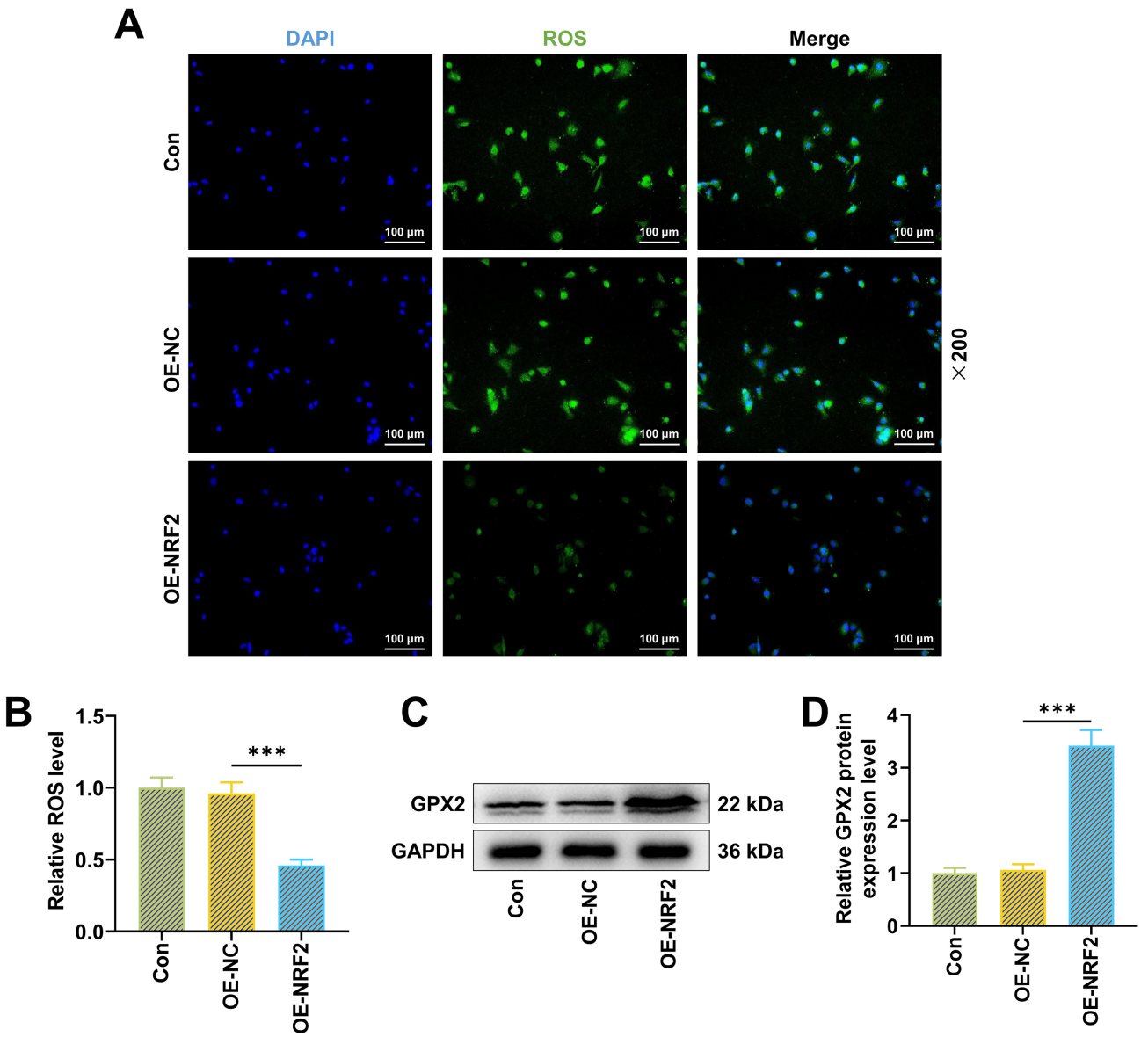

Fig. 2. Effect of *NRF2* overexpression on ROS level and GPX2 protein expression in erastin-treated B16 cells. (A–D) In B16 cells receiving 24-h treatment with 5 μM erastin, ROS level (2,7-dichlorodihydrofluorescein diacetate (DCFH-DA) staining) (×200 magnification, scale bar: 100 μm) (A,B), and GPX2 expression (western blot, *GAPDH* as the internal control) were tested (C,D). n = 3. $^{***}p < 0.001$. GPX2, glutathione peroxidase 2; ROS, reactive oxygen species.

was attenuated by *GPX2* knockdown (Fig. 4A,B, $p < 0.01$). In addition, PD-L1 showed reduced expression in Si-*GPX2*-transfected cells (Fig. 4A,B, $p < 0.01$) after erastin treatment, while *NRF2* overexpression counteracted this effect of *GPX2* knockdown (Fig. 4A,B, $p < 0.001$).

GPX2 Knockdown Restored NRF2 Overexpression-Promoted Apoptosis in CD8$^+$ T Cells

The transfected B16 cells were then co-cultured with CD8$^+$ T cells to assess B16 cell immune escape. *NRF2* overexpression in B16 cells promoted, while *GPX2* knockdown repressed the apoptosis of CD8$^+$ T cells (Fig. 4C,D, $p < 0.001$). The effects of *GPX2* knockdown and *NRF2* overexpression on apoptosis of CD8$^+$ T cells were mutually counteracted (Fig. 4C,D, $p < 0.001$).

Blocking PD-1/PD-L1 Attenuated NRF2 Overexpression-Inhibited Infiltration of CD8$^+$ T Cells in Subcutaneous Xenograft Tumor Mice

To investigate whether the impact of *NRF2*/*GPX2* depended on the mediation of PD-1/PD-L1, we constructed a subcutaneous xenograft tumor model and injected PD-1 or PD-L1 antibody into model mice. CD8$^+$ T cell infiltration was irreplaceable for immunoreaction in tumors [31]. By IHC, we observed that *NRF2* overexpression lowered infil-

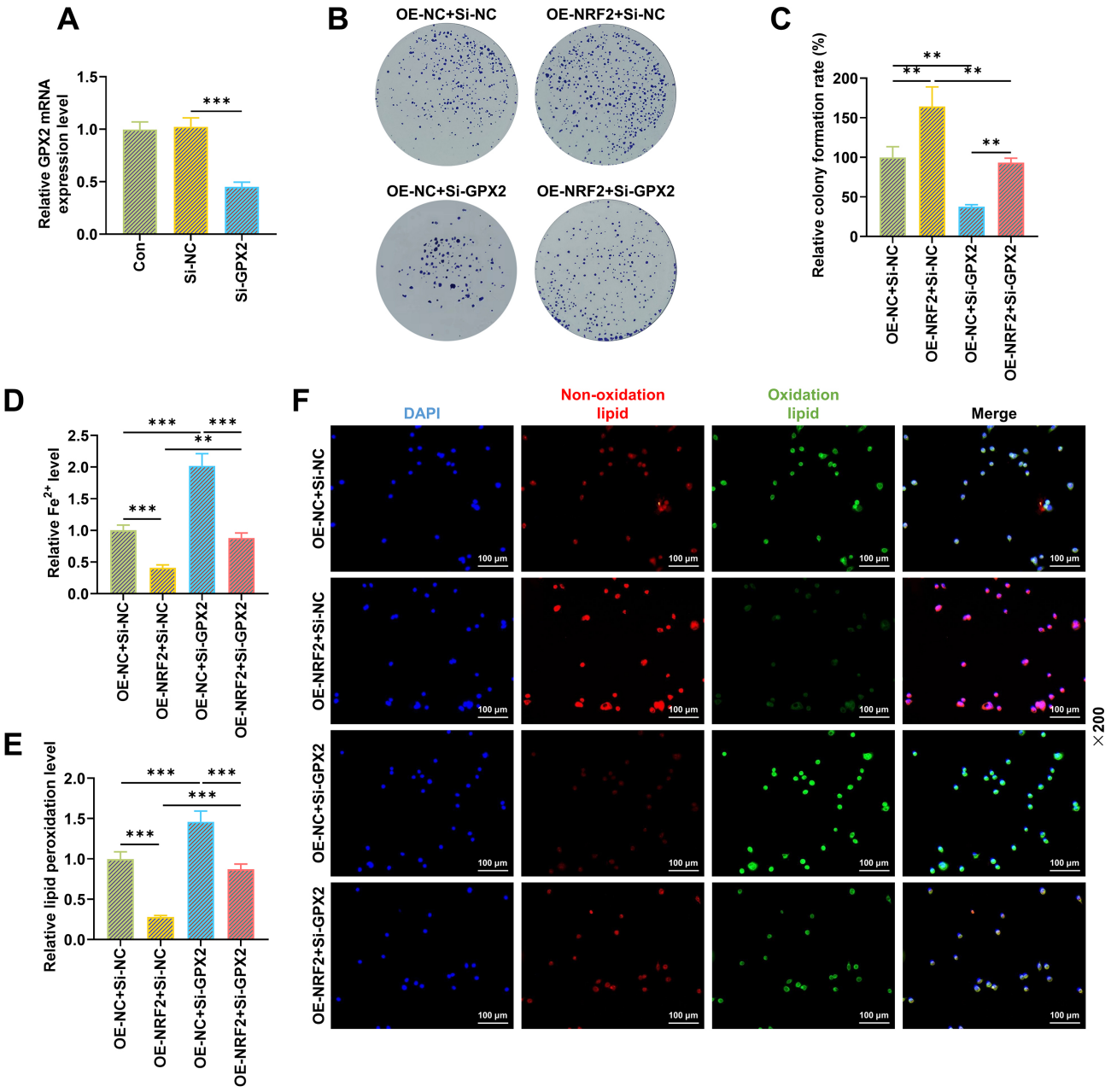

Fig. 3. *GPX2* knockdown reversed the effects of *NRF2* overexpression on colony formation and ferroptosis in erastin-treated B16 cells. (A) Transfection efficiency after B16 cells was transfected with Si-*GPX2* (qRT-PCR, *GAPDH* as internal control). (B–F) In B16 cells receiving 24-h treatment with 5 μM erastin, colony number (colony formation assay) (B,C), Fe^{2+} level (iron assay kit) (D), and lipid peroxidation (C11-BODIPY staining) were determined (×200 magnification, scale bar: 100 μm) (E,F). n = 3. $^{**}p < 0.01$, $^{***}p < 0.001$. Si-*GPX2*, small interfering RNA against GPX2.

tration of $CD8^+$ T cells into tumor tissues of model mice (Fig. 4E,F, $p < 0.01$), which was attenuated following the injection of PD-1 or PD-L1 antibody (Fig. 4E,F, $p < 0.01$). Based on the above findings, we inferred that *NRF2*/*GPX2* was involved in PD-1/PD-L1-mediated immune escape of B16 cells.

Discussion

NRF2 has been reported to have carcinogenic or antitumor activity in different cancer models [32]. In melanoma, *NRF2* was previously confirmed to modulate innate immune responses and oxidative stress [33]. Of note, oxidative stress and antioxidant responses are conducive to melanoma development [34]. A previous study showed that *NRF2* enhances melanoma malignancy via blocking differ-

Journal of
BIOLOGICAL REGULATORS
and Homeostatic Agents

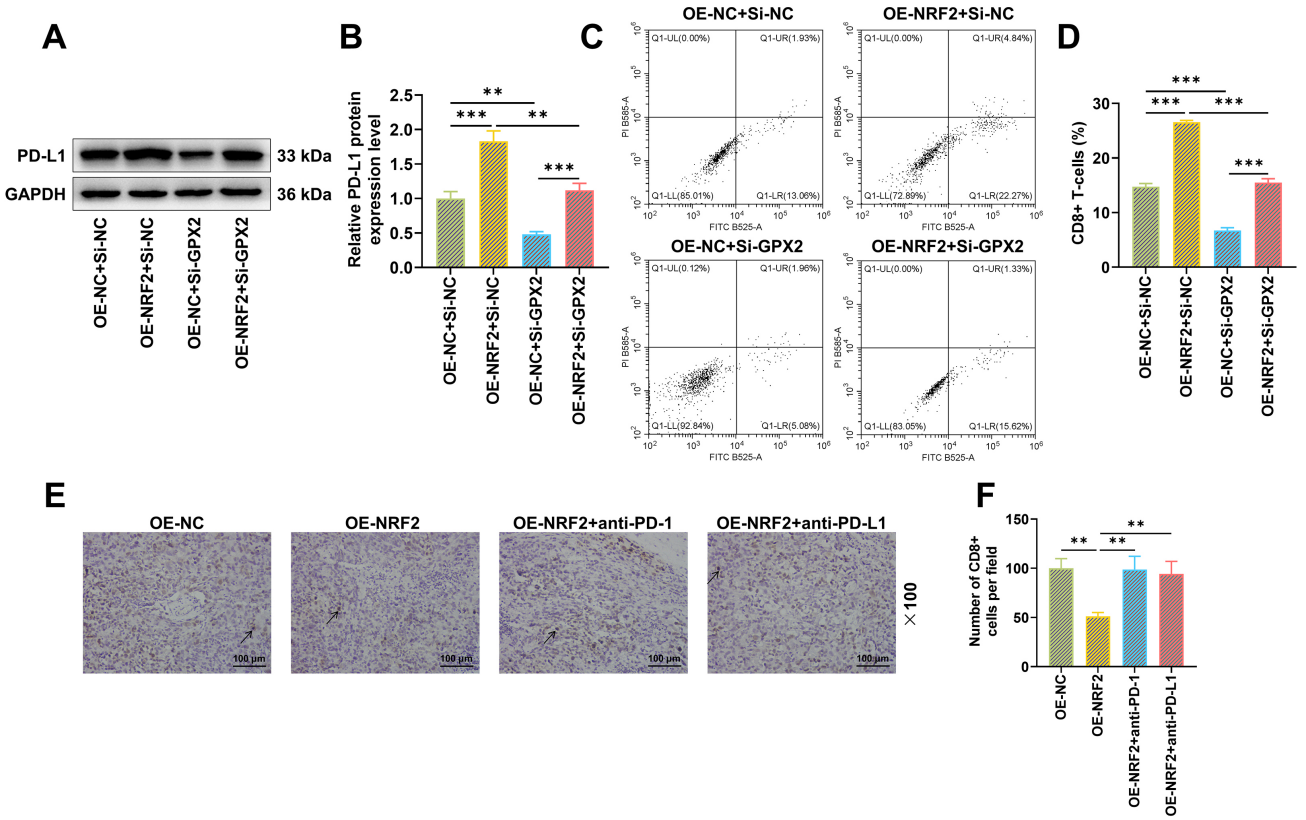

Fig. 4. Effects of *NRF2*/*GPX2* on PD-1/PD-L1 pathway-related immune escape in melanoma. (A,B) PD-L1 expression in B16 cells was transfected with *NRF2* overexpression plasmid and/or Si-*GPX2* plasmid and treated with 5 μM erastin for 24 h (western blot, *GAPDH* as internal control). (C,D) $CD8^+$ T cell apoptosis following co-culture of B16 cells and $CD8^+$ T cells (flow cytometry). (E,F) $CD8^+$ T cell infiltration into tumors after subcutaneous xenograft tumors was established and mice were injected with PD-1 or PD-L1 antibody (IHC), arrow: the inflammatory infiltration (×100 magnification, scale bar: 100 μm). n = 3. $^{**}p < 0.01$, $^{***}p < 0.001$. PD-L1, CD274 molecule; PD-1, programmed cell death 1; IHC, immunohistochemistry.

entiation and increasing *COX2* expression [35]. Further, *NRF2* participates vigorously in ferroptosis of melanoma [23,36,37]. Ferroptosis, a form of cell death, results from massive accumulation of Fe^{2+} and lipid peroxidation [38]. Erastin is widely applied as a ferroptosis inducer in tumor researches [39,40]. The activated *NRF2*-dependent antioxidative mechanism in ferroptosis has been identified in melanoma [23]. *miR-130b-3p* may inhibit ferroptosis in melanoma cells by means of the Dickkopf1 (*DKK1*)-mediated *NRF2*/heme oxygenase 1 (HO-1) pathway [37]. In this study, we found that *NRF2* overexpression enhanced proliferation, but inhibited levels of Fe^{2+}, lipid peroxidation, and ROS in erastin-treated B16 cells, indicating that *NRF2* overexpression reversed erastin-induced ferroptosis of melanoma and reduced ferroptosis in melanoma.

Furthermore, in this study, *GPX2* expression was upregulated by *NRF2* overexpression in erastin-treated B16 cells, suggesting that *GPX2* might participate in the regulation of *NRF2* on ferroptosis of melanoma cells. *GPX2* is regarded as a ferroptosis-related gene and is implicated in tumor prognosis [41,42]. Intriguingly, the GPX2 gene demonstrates low expression in melanoma cell lines, and is a risk factor for overall survival [43]. A previous study showed that GPX2 expression is regulated by several pathways, including NRF2 [44]. The regulation of *NRF2* on *GPX2* has been previously identified [45,46]. In addition, *GPX2* is a metabolic driver of the tumor immune checkpoint inhibitor response and its expression is intimately correlated with *NRF2* activation in assorted cancers [24]. We constructed *GPX2*-deficient B16 cells and found that *GPX2* knockdown reversed the effects of *NRF2* overexpression on both proliferation and ferroptosis. We then demonstrated that *NRF2* inhibited ferroptosis by upregulating *GPX2* in melanoma. However, Hiller *et al*. [47] showed that in dextran sulfate sodium-treated *NRF2* knockout mice, *GPX2* expression remained upregulated during recovery and independent of *NRF2*. More experiments are needed to verify the regulation between *NRF2* and *GPX2* in different diseases.

In addition, *NRF2* promotes immune escape in liver hepatocellular carcinoma and glioma [16,17]. *GPX2* overexpression is also regarded as a potential effector of immune escape in tumors [24]. Moreover, the PD-1/PD-L1 axis can contribute to immune escape in various tumors

through regulation of T-cell activity, activation of antigen-specific T cell apoptosis, and inhibition of regulatory T cell apoptosis [48,49]. A previous study showed that in clinical specimens and animal models, *NRF2* mediates PD-L1 expression [50]. Inhibition of the Nrf2-PD-L1 signaling pathway can augment the efficacy of oxaliplatin in patients with colon cancer [51]. Interestingly, recent studies reported that ferroptosis can mediate the effect of anti-PD-1 immunotherapy in melanoma [23,30]. In this study, we confirmed increased expression of PD-L1 in *NRF2*-overexpressing B16 cells following erastin treatment, and such increment was restored by *GPX2* knockdown. Therefore, we speculated that the *NRF2*/*GPX2* axis activated PD-1/PD-L1-mediated immune escape in melanoma.

NRF2 stimulates PD-L1 transcription, targeting and inhibition, which is an alternative route to suppress PD-1/PD-L1, induce tumor infiltration by $CD4^+$ and $CD8^+$ T lymphocytes, consequentially blocking melanoma growth [52]. $CD8^+$ T cells are essential for adoptive immunity and are vital immune cells for targeting cancer [53]. To verify our hypothesis, we performed *in vitro* co-culture of B16 cells and $CD8^+$ T cells to mimic the tumor immune microenvironment in melanoma. Data showed that *NRF2* overexpression in B16 cells promoted the apoptosis of $CD8^+$ T cells, while *GPX2* knockdown did the opposite. *GPX2* knockdown mitigated the promoting effects of *NRF2* overexpression. Further, we observed that *NRF2* overexpression significantly reduced the infiltration of $CD8^+$ T cells into tumor tissues of model mice, suggesting that *NRF2* overexpression induced an immunosuppressive microenvironment in tumor tissues, which was relieved by blocking PD-1 or PD-L1. Thus, it can be concluded that the *NRF2*/*GPX2* axis exerts a regulatory effect on mediated immune escape in melanoma.

We demonstrated that the *NRF2*/*GPX2* axis inhibits mediated immune escape in melanoma via activating PD-1/PD-L1 pathway, providing a potential new strategy for melanoma immunotherapy. However, there are some limitations in this study. (1) B16, a mouse melanoma cell line, may inaccurately represent human skin cancer biology; (2) The association between iron-related cell death and tumor immunity is not fully understood; (3) We purposefully selected a gene which may have excluded other important genes for melanoma; (4) This study only predicted short-term outcomes, thereby limiting possible conclusions regarding long-term outcomes; (5) Our study results have not been verified by clinical experiments. Therefore, follow-up research, long-term animal model studies, and clinical trials are necessary.

Conclusion

Taken together, this study demonstrates that the *NRF2*/*GPX2* axis inhibits erastin-induced ferroptosis of melanoma cells, and enhances immune escape in an immune microenvironment in melanoma by activating the PD-1/PD-L1 pathway. These findings may provide references for targeted therapy against melanoma.

Availability of Data and Materials

The analyzed data sets generated during the study are available from the corresponding author on reasonable request.

Author Contributions

Substantial contributions to conception and design: LW, ML. Data acquisition, data analysis and interpretation: HYH. Drafting the article or critically revising it for important intellectual content: All authors. Final approval of the version to be published: All authors. Agreement to be accountable for all aspects of the work in ensuring that questions related to the accuracy or integrity of the work are appropriately investigated and resolved: All authors.

Ethics Approval and Consent to Participate

All animal experiments were approved by the Zhejiang Province Center for Laboratory Animals, Institutional of Animal Care and Use Committee (No. ZJCLA-IACUC-20020175).

Acknowledgment

Not applicable.

Funding

This research received no external funding.

Conflict of Interest

The authors declare no conflict of interest.

Supplementary Material

Supplementary material associated with this article can be found, in the online version, at https://doi.org/10.23812/j.biol.regul.homeost.agents.20243805.347.

References

[1] Perez-Valle A, Abad-García B, Fresnedo O, Barreda-Gómez G, Aspichueta P, Asumendi A, *et al*. A UHPLC-Mass Spectrometry View of Human Melanocytic Cells Uncovers Potential Lipid Biomarkers of Melanoma. International Journal of Molecular Sciences. 2021; 22: 12061.

[2] Lopes J, Rodrigues CMP, Gaspar MM, Reis CP. Melanoma Management: From Epidemiology to Treatment and Latest Advances. Cancers. 2022; 14: 4652.

[3] Villani A, Potestio L, Fabbrocini G, Troncone G, Malapelle U, Scalvenzi M. The Treatment of Advanced Melanoma: Ther-

Journal of
BIOLOGICAL REGULATORS
and Homeostatic Agents

apeutic Update. International Journal of Molecular Sciences. 2022; 23: 6388.

[4] Jin S, Mishra-Kalyani PS, Sridhara R. Unresectable and Metastatic Melanoma of the Skin: Literature Review of Clinical Trials and Efficacy Endpoints Since 2000. Therapeutic Innovation & Regulatory Science. 2019; 53: 59–70.

[5] Wang W, Green M, Choi JE, Gijón M, Kennedy PD, Johnson JK, *et al*. CD8$^+$ T cells regulate tumour ferroptosis during cancer immunotherapy. Nature. 2019; 569: 270–274.

[6] Khorsandi K, Esfahani H, Ghamsari SK, Lakhshehei P. Targeting ferroptosis in melanoma: cancer therapeutics. Cell Communication and Signaling: CCS. 2023; 21: 337.

[7] Wang Z, Jin D, Ma D, Ji C, Wu W, Xu L, *et al*. Ferroptosis suppressed the growth of melanoma that may be related to DNA damage. Dermatologic Therapy. 2019; 32: e12921.

[8] Jiang Z, Lim SO, Yan M, Hsu JL, Yao J, Wei Y, *et al*. TYRO3 induces anti-PD-1/PD-L1 therapy resistance by limiting innate immunity and tumoral ferroptosis. The Journal of Clinical Investigation. 2021; 131: e139434.

[9] Tonelli C, Chio IIC, Tuveson DA. Transcriptional Regulation by Nrf2. Antioxidants & Redox Signaling. 2018; 29: 1727–1745.

[10] G Bardallo R, Panisello-Roselló A, Sanchez-Nuno S, Alva N, Roselló-Catafau J, Carbonell T. Nrf2 and oxidative stress in liver ischemia/reperfusion injury. The FEBS Journal. 2022; 289: 5463–5479.

[11] Ulasov AV, Rosenkranz AA, Georgiev GP, Sobolev AS. Nrf2/Keap1/ARE signaling: Towards specific regulation. Life Sciences. 2022; 291: 120111.

[12] Chen QM. Nrf2 for protection against oxidant generation and mitochondrial damage in cardiac injury. Free Radical Biology & Medicine. 2022; 179: 133–143.

[13] Vallion R, Kerdine-Römer S. Regulation of the immune response to contact sensitizers by Nrf2. Contact Dermatitis. 2022; 87: 13–19.

[14] van der Horst D, Carter-Timofte ME, van Grevenynghe J, Laguette N, Dinkova-Kostova AT, Olagnier D. Regulation of innate immunity by Nrf2. Current Opinion in Immunology. 2022; 78: 102247.

[15] Yang W, Wang Y, Zhang P, Sun X, Chen X, Yu J, *et al*. Immune-responsive gene 1 protects against liver injury caused by concanavalin A via the activation Nrf2/HO-1 pathway and inhibition of ROS activation pathways. Free Radical Biology & Medicine. 2022; 182: 108–118.

[16] Hu J, Yang L, Peng X, Mao M, Liu X, Song J, *et al*. ALDH2 Hampers Immune Escape in Liver Hepatocellular Carcinoma through ROS/Nrf2-mediated Autophagy. Inflammation. 2022; 45: 2309–2324.

[17] Wang J, Liu P, Xin S, Wang Z, Li J. Nrf2 suppresses the function of dendritic cells to facilitate the immune escape of glioma cells. Experimental Cell Research. 2017; 360: 66–73.

[18] Wu Q, Wang X, Nepovimova E, Miron A, Liu Q, Wang Y, *et al*. Trichothecenes: immunomodulatory effects, mechanisms, and anti-cancer potential. Archives of Toxicology. 2017; 91: 3737–3785.

[19] Rosenthal R, Cadieux EL, Salgado R, Bakir MA, Moore DA, Hiley CT, *et al*. Neoantigen-directed immune escape in lung cancer evolution. Nature. 2019; 567: 479–485.

[20] Cozza G, Rossetto M, Bosello-Travain V, Maiorino M, Roveri A, Toppo S, *et al*. Glutathione peroxidase 4-catalyzed reduction of lipid hydroperoxides in membranes: The polar head of membrane phospholipids binds the enzyme and addresses the fatty acid hydroperoxide group toward the redox center. Free Radical Biology & Medicine. 2017; 112: 1–11.

[21] Zhou SY, Cui GZ, Yan XL, Wang X, Qu Y, Guo ZN, *et al*. Mechanism of Ferroptosis and Its Relationships With Other Types of Programmed Cell Death: Insights for Potential Interventions After Intracerebral Hemorrhage. Frontiers in Neuroscience. 2020; 14: 589042.

[22] Huang GJ, Liu HB. Identification and validation of ferroptosis-related genes for chronic rhinosinusitis with nasal polyps. European Archives of Oto-rhino-laryngology: Official Journal of the European Federation of Oto-Rhino-Laryngological Societies (EUFOS): Affiliated with the German Society for Oto-Rhino-Laryngology - Head and Neck Surgery. 2023; 280: 1501–1508.

[23] Wang S, Yi X, Wu Z, Guo S, Dai W, Wang H, *et al*. CAMKK2 Defines Ferroptosis Sensitivity of Melanoma Cells by Regulating AMPK–NRF2 Pathway. The Journal of Investigative Dermatology. 2022; 142: 189–200.e8.

[24] Ahmed KM, Veeramachaneni R, Deng D, Putluri N, Putluri V, Cardenas MF, *et al*. Glutathione peroxidase 2 is a metabolic driver of the tumor immune microenvironment and immune checkpoint inhibitor response. Journal for Immunotherapy of Cancer. 2022; 10: e004752.

[25] Brigelius-Flohé R, Kipp AP. Physiological functions of GPx2 and its role in inflammation-triggered carcinogenesis. Annals of the New York Academy of Sciences. 2012; 1259: 19–25.

[26] Livak KJ, Schmittgen TD. Analysis of relative gene expression data using real-time quantitative PCR and the 2(-Delta Delta C(T)) Method. Methods (San Diego, Calif.). 2001; 25: 402–408.

[27] Yang Y, Luo M, Zhang K, Zhang J, Gao T, Connell DO, *et al*. Nedd4 ubiquitylates VDAC2/3 to suppress erastin-induced ferroptosis in melanoma. Nature Communications. 2020; 11: 433.

[28] Yang J, Mo J, Dai J, Ye C, Cen W, Zheng X, *et al*. Cetuximab promotes RSL3-induced ferroptosis by suppressing the Nrf2/HO-1 signalling pathway in KRAS mutant colorectal cancer. Cell Death & Disease. 2021; 12: 1079.

[29] Wei CY, Zhu MX, Lu NH, Liu JQ, Yang YW, Zhang Y, *et al*. Circular RNA circ_0020710 drives tumor progression and immune evasion by regulating the miR-370-3p/CXCL12 axis in melanoma. Molecular Cancer. 2020; 19: 84.

[30] Friedmann Angeli JP, Meierjohann S. NRF2-dependent stress defense in tumor antioxidant control and immune evasion. Pigment Cell & Melanoma Research. 2021; 34: 268–279.

[31] Lu T, Zhang J, Lu S, Yang F, Gan L, Wu X, *et al*. Endosialin-positive tumor-derived pericytes promote tumor progression through impeding the infiltration of CD8$^+$ T cells in clear cell renal cell carcinoma. Cancer Immunology, Immunotherapy: CII. 2023; 72: 1739–1750.

[32] Rojo de la Vega M, Chapman E, Zhang DD. NRF2 and the Hallmarks of Cancer. Cancer Cell. 2018; 34: 21–43.

[33] He CH, Gong P, Hu B, Stewart D, Choi ME, Choi AM, *et al*. Identification of activating transcription factor 4 (ATF4) as an Nrf2-interacting protein. Implication for heme oxygenase-1 gene regulation. The Journal of Biological Chemistry. 2001; 276: 20858–20865.

[34] Arslanbaeva LR, Santoro MM. Adaptive redox homeostasis in cutaneous melanoma. Redox Biology. 2020; 37: 101753.

[35] Jessen C, Kreß JKC, Baluapuri A, Hufnagel A, Schmitz W, Kneitz S, *et al*. The transcription factor NRF2 enhances melanoma malignancy by blocking differentiation and inducing COX2 expression. Oncogene. 2020; 39: 6841–6855.

[36] Feng S, Zhou Y, Huang H, Lin Y, Zeng Y, Han S, *et al*. Nobiletin Induces Ferroptosis in Human Skin Melanoma Cells Through the GSK3β-Mediated Keap1/Nrf2/HO-1 Signalling Pathway. Frontiers in Genetics. 2022; 13: 865073.

[37] Liao Y, Jia X, Ren Y, Deji Z, Gesang Y, Ning N, *et al*. Suppressive role of microRNA-130b-3p in ferroptosis in melanoma cells correlates with DKK1 inhibition and Nrf2-HO-1 pathway activation. Human Cell. 2021; 34: 1532–1544.

[38] Zhang HL, Hu BX, Li ZL, Du T, Shan JL, Ye ZP, *et al*. PKCβII phosphorylates ACSL4 to amplify lipid peroxidation to induce ferroptosis. Nature Cell Biology. 2022; 24: 88–98.

[39] Li Y, Zeng X, Lu D, Yin M, Shan M, Gao Y. Erastin induces ferroptosis via ferroportin-mediated iron accumulation in endometriosis. Human Reproduction (Oxford, England). 2021; 36: 951–964.

[40] Zhou HH, Chen X, Cai LY, Nan XW, Chen JH, Chen XX, *et al*. Erastin Reverses ABCB1-Mediated Docetaxel Resistance in Ovarian Cancer. Frontiers in Oncology. 2019; 9: 1398.

[41] Luo L, Yao X, Xiang J, Huang F, Luo H. Identification of ferroptosis-related genes for overall survival prediction in hepatocellular carcinoma. Scientific Reports. 2022; 12: 10007.

[42] Tian Q, Zhou Y, Zhu L, Gao H, Yang J. Development and Validation of a Ferroptosis-Related Gene Signature for Overall Survival Prediction in Lung Adenocarcinoma. Frontiers in Cell and Developmental Biology. 2021; 9: 684259.

[43] Ping S, Wang S, Zhao Y, He J, Li G, Li D, *et al*. Identification and validation of a ferroptosis-related gene signature for predicting survival in skin cutaneous melanoma. Cancer Medicine. 2022; 11: 3529–3541.

[44] Esworthy RS, Doroshow JH, Chu FF. The beginning of GPX2 and 30 years later. Free Radical Biology & Medicine. 2022; 188: 419–433.

[45] Horniblow RD, Pathak P, Balacco DL, Acharjee A, Lles E, Gkoutos G, *et al*. Iron-mediated epigenetic activation of NRF2 targets. The Journal of Nutritional Biochemistry. 2022; 101: 108929.

[46] Singh G, Haileselassie Y, Ji AR, Maecker HT, Sinha SR, Brim H, *et al*. Protective Effect of Saffron in Mouse Colitis Models Through Immune Modulation. Digestive Diseases and Sciences. 2022; 67: 2922–2935.

[47] Hiller F, Besselt K, Deubel S, Brigelius-Flohé R, Kipp AP. GPx2 Induction Is Mediated Through STAT Transcription Factors During Acute Colitis. Inflammatory Bowel Diseases. 2015; 21: 2078–2089.

[48] Han Y, Liu D, Li L. PD-1/PD-L1 pathway: current researches in cancer. American Journal of Cancer Research. 2020; 10: 727–742.

[49] Jiang X, Wang J, Deng X, Xiong F, Ge J, Xiang B, *et al*. Role of the tumor microenvironment in PD-L1/PD-1-mediated tumor immune escape. Molecular Cancer. 2019; 18: 10.

[50] Zhang D, Man D, Lu J, Jiang Y, Ding B, Su R, *et al*. Mitochondrial TSPO Promotes Hepatocellular Carcinoma Progression through Ferroptosis Inhibition and Immune Evasion. Advanced Science (Weinheim, Baden-Wurttemberg, Germany). 2023; 10: e2206669.

[51] Payandeh Z, Pirpour Tazehkand A, Mansoori B, Khaze V, Asadi M, Baradaran B, *et al*. The Impact of Nrf2 Silencing on Nrf2-PD-L1 Axis to Overcome Oxaliplatin Resistance and Migration in Colon Cancer Cells. Avicenna Journal of Medical Biotechnology. 2021; 13: 116–122.

[52] Zhu B, Tang L, Chen S, Yin C, Peng S, Li X, *et al*. Targeting the upstream transcriptional activator of PD-L1 as an alternative strategy in melanoma therapy. Oncogene. 2018; 37: 4941–4954.

[53] Farhood B, Najafi M, Mortezaee K. $CD8^+$ cytotoxic T lymphocytes in cancer immunotherapy: A review. Journal of Cellular Physiology. 2019; 234: 8509–8521.